

NEURAL NETWORK MODEL OF THE MULTI-MODE ANOMALOUS TRANSPORT MODULE

Real-time-capable Machine-learning-based Accelerated Model for Transport Simulations

S.M. MOROSOHK, A. PAJARES, T. RAFIQ, E. SCHUSTER
Lehigh University
Bethlehem, Pennsylvania 18015, USA
Email: morosohk@lehigh.edu

Abstract

A neural network version of the Multi-Mode Anomalous Transport Module, known as MMMnet, has been developed to calculate plasma turbulent diffusivities in DIII-D with a calculation time suitable for control applications. MMMnet uses a simple artificial neural network structure to predict the ion thermal, electron thermal, and toroidal momentum diffusivities while reproducing Multi-Mode Model (MMM) data with good accuracy and keeping the calculation time as a fraction of that associated with MMM. Model-based control techniques require models with fast calculation times, making many existing physics-oriented predictive codes unsuitable. The control-oriented predictive code COTSIM (Control-Oriented Transport Simulator) has been developed to calculate the most significant plasma dynamics in response to the different actuators while running at a speed useful for control design. In order to achieve this calculation speed, COTSIM relies on scaling laws and control-level models. Replacing some of these scaling laws and control-level models with neural network versions of more complex physics-level models has the potential of increasing the range of validity and the level of accuracy of COTSIM without compromising its computational speed. In this work, MMMnet is integrated into COTSIM to improve the turbulent diffusivity predictions, which will in turn improve the prediction accuracy associated with the dynamics of many plasma properties.

1. INTRODUCTION

In order for tokamak plasmas to achieve both stable operation and high performance, the 1D spatial distributions of plasma parameters such as density, temperature, current, and momentum must be carefully controlled. The evolution of these profiles in time is described by a system of nonlinear transport equations that are too complicated to be modeled from first principles with reasonable calculation times. Reduced physics-based models are available, but they are still too computationally intensive to be well suited for control applications.

Model-based control applications require response models with fast (e.g., for closed-loop offline simulations) to extremely fast (e.g., for real-time control and estimation) calculation times, making well-established physics-oriented predictive transport codes challenging or impossible to use. Instead, control-oriented models with significantly faster calculation times must be developed; however, this speed often comes with a cost. Reducing physics models to the point that they run at the required speeds can also reduce accuracy beyond the point where the model is useful. Empirical scaling laws can achieve high levels of accuracy, but may only be valid for specific plasma scenarios. Machine learning models have the uncommon ability to meet all three goals: high levels of accuracy, fast calculation times, and applicability to a broader range of plasma scenarios. Recently, neural-network versions of a number of physics-based codes for both transport [1, 2] and sources [3, 4] have been developed, which significantly reduce the calculation time required while maintaining relatively high prediction accuracies across many different scenarios. Inspired by these recent developments on machine-learning-based plasma-response modeling, a neural network that reproduces the predictions of the Multi-Mode Model (MMM) [5] for anomalous transport has been developed for DIII-D.

The MMMnet model has been trained to reproduce the calculation of the ion thermal, electron thermal, and toroidal momentum turbulent diffusivities. A simple artificial neural network structure was used with three hidden layers and 100 nodes per hidden layer. Five separate networks were trained with different initializations of the weights; the final prediction returned is the average of the five predictions. A low standard deviation between the predictions indicates that the training effectively eliminates any randomness introduced by the initial weights. Training data was generated by calling 1000 predictive TRANSP runs based on 83 different DIII-D shots and using MMM as the transport model. Instead of relying on a convolutional neural network to handle spatially-varying data, principle component analysis was applied to the plasma profiles to reduce the amount of data used

to describe each profile. This reduced the number of input and output nodes in the network, thereby limiting the network complexity and calculation time.

The **Control Oriented Transport Simulator (COTSIM)** [6] is a 1D transport code designed to run at speeds useful for control applications. It uses either a prescribed MHD equilibrium or a fixed-boundary analytical solver, although the coupling with a free-boundary numerical solver is currently in progress. It uses a modular configuration which allows the user to easily choose from transport and source models of varying complexities, ranging from empirical scalings to reduced analytical models to machine learning models. A neural network version of NUBEAM [4] is already available to calculate beam driven current, heating, and torque. Depending on the models chosen, COTSIM takes between a fraction of a second and several seconds to simulate a full DIII-D discharge. In this work, the neural network version of MMM is integrated into COTSIM to enhance its fast prediction capabilities.

This paper is organized as follows. In Section 2, the process used to obtain the dataset needed to train and evaluate the neural network model is described. In Section 3, the method used to process the data and determine the topology and training parameters of the model is explained. In Section 4, the results of the final neural network model are presented. In Section 5, the neural network is integrated into COTSIM and predictive-simulation results are shown. In Section 6, conclusions and plans for future work are discussed.

2. DATASET DEVELOPMENT

The input data used in this work was taken from a set of 1000 predictive TRANSP runs using MMM as the transport model and evolving the electron and ion temperature profiles. This ensures that the inputs to MMM are in a physically reasonable range for DIII-D Deuterium plasmas. The TRANSP runs are based on 83 different shots from the 2018 DIII-D campaign. For each TRANSP run, the mean effective charge (Z_{eff}) was randomly assigned a value between 1.5 and 5, the edge neutral density ($n_{0,out}$) was randomly assigned a value between 5×10^{10} and $1 \times 10^{13.5} cm^{-3}$, and the anomalous fast ion diffusivity (D_f) was assigned either a classical, flat, or peaked shape and a maximum value between 1 and 50,000 cm^2/s . Changing the values of Z_{eff} directly effects the calculation of the diffusivities by MMM. Changing $n_{0,out}$ and D_f changes the calculation of the effects of neutral beam injection by NUBEAM, which changes the temperature inputs to MMM and thus indirectly alters the calculated diffusivities. By this process, the original 83 shots are expanded to 1000 TRANSP runs, or 201,612 total time steps in the dataset.

The total dataset is then divided into three subsets used for training, validation, and testing. One of the main concerns when training a neural network is that the network could be learning the exact training data more than the underlying function which describes the data; this issue is referred to as overfitting. If this is the case, for any point that was not included in the original training set, the network would be unable to generalize and would produce less useful predictions. In order to check for this, a portion of the data is held back during training. The training set, made up of 80% of the TRANSP runs in the total dataset, is what the neural network actually sees during the training process. 10% of the TRANSP runs go into the validation set, which is used during the parameter tuning process to determine the values of the manually assigned network parameters, or hyperparameters (see Section 3). The remaining 10% of the TRANSP runs make up the testing set, and are used to assess the performance of the final model.

2.1. Model Inputs and Outputs

The inputs used in this network are most of the inputs used by the standalone version of MMM. The parallel velocity was left out because it was assumed to be equal to the toroidal velocity, and the mean atomic mass of ions was left out because that information could be derived from the average charge and the atomic mass of impurities. This ensured that the network had all of the data it needed to generate diffusivity predictions. The inputs are listed in Table 1. For some of the input quantities, the normalized gradient is also used and is treated as a separate input, as also indicated in Table 1. Fig. 1 shows the range of each input in the training dataset. Because machine learning models cannot extrapolate, this gives a lower-dimensional representation of the range for which the neural network predictions will be valid. The outputs of the neural network are ion thermal (χ_i), electron thermal (χ_e), and toroidal momentum (χ_ϕ) diffusivities, all measured in m^2/s . These profiles use 15, 14, and 12 PCA (principle component analysis) modes (see Section 3.1), respectively. The value of these outputs is only reported in these TRANSP runs up to a spatial location of $\hat{\rho} = 0.8$, so MMMnet is only trained to produce valid predictions in that region.

Table 1: Inputs to the final neural network model.

Inputs						
Symbol	Name	Units	PCA Modes	Gradient	Gradient PCA Modes	
Z_{imp}	Average charge of impurities					
A_{imp}	Average atomic mass of impurities	amu				
Z_{eff}	Mean effective charge		1			
κ	Elongation		4			
R	Major radius	m	4			
$RMAJM$	Midplane flux surface radii	m	1			
r	Minor radius	m	4			
B_t	Toroidal magnetic field	T	2			
n_e	Electron density	m^{-3}	5	✓		2
n_i	Ion density	m^{-3}	6	✓		2
n_h	Hydrogenic ion density	m^{-3}	5	✓		2
n_z	Impurity density	m^{-3}	5	✓		2
n_f	Fast ion density	m^{-3}	2			
T_e	Electron temperature	keV	4	✓		2
T_i	Ion temperature	keV	4	✓		2
q	Safety factor		5	✓		7
ω_{ExB}	ExB shear	rad/s	8			
v_ϕ	Toroidal velocity	m/s	4	✓		7
v_θ	Poloidal velocity	cm/s	1	✓		6

3. MODEL STRUCTURE

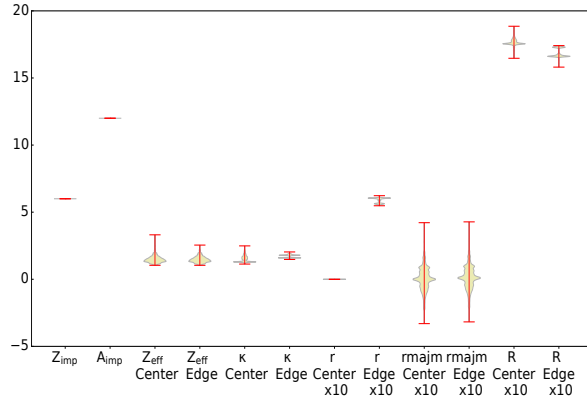
3.1. Data Preprocessing

When predicting spatially-varying data, a typical approach is to use a convolutional neural network (CNN). This technique is well-suited to datasets with two or three spatial dimensions and is often used in image recognition and computer vision applications. However, it is a more complicated architecture than the multi-layer perceptron (MLP), and can therefore have slightly higher calculation times. Given the goal of developing a network with as fast a prediction time as possible, it was decided to use an MLP in this work. In order to use this simpler approach, each profile must be reduced to a set of scalar points. This can be accomplished using a principle component analysis (PCA), which projects each profile, including gradients, onto a set of basis functions and determines how much of the total variance in the data each basis function accounts for. In this work, the PCA for each profile and gradient includes every basis function that explains at least 0.1% of the variance in the data. This ensures that the basis functions that are retained add up to at least 99.5% of the total variance. The number of basis functions retained for each profile, and gradient if the gradient is included, is in Table 1. It is important to point out that the PCA for each profile is derived from the training dataset, and is therefore only valid for profiles in the same range as those in the training data. Just as the neural network cannot extrapolate to regions far from any training data point, the PCA cannot accurately deconstruct and reconstruct a profile that is significantly different from any profile in the training data.

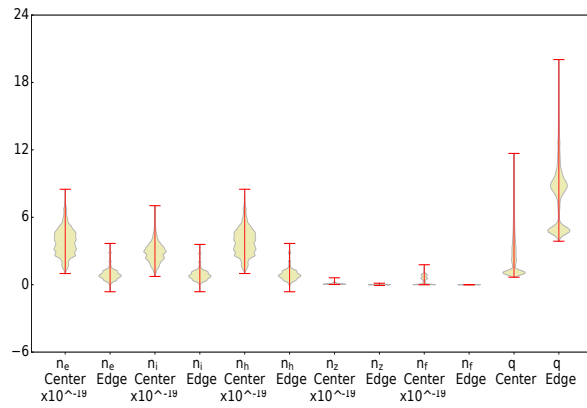
Before the data can be fed to the neural network, each input and output is standardized to a mean of 0 and a standard deviation of 1. This ensures that all inputs are given equal weight in the prediction, that inputs such as densities with a higher absolute value do not overpower the other inputs, and that all outputs are given equal weight when calculating the loss function. For each prediction the neural network makes, the profile data is reduced to a set of scalars through the PCA, all the inputs are standardized, the neural network makes its prediction, the network outputs go through the reverse of the standardization process, and the final profiles are reconstructed by the PCA.

3.2. Determination of Hyperparameters

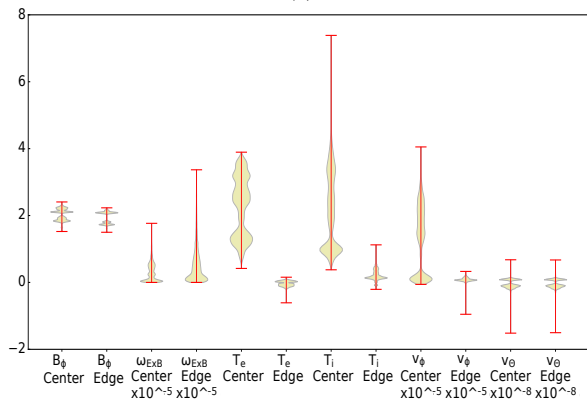
The term hyperparameters refers to all of the network parameters which are not learned during the training process. These include the structure of the network and length of the training process, among others. It is up to the person training the neural network to choose values of these parameters that yield good results. Methods of determining these parameters include genetic-algorithm optimization [7] and Bayesian optimization [8]. However, the most



(a)



(b)



(c)

Figure 1: Range of inputs in the training dataset. x -axes show quantities, y -axes reflect the range of values of each quantity, and the width of the green space represents the frequency that that value is seen in the training dataset.

common approach is still to conduct a grid search, or a brute force testing of different hyperparameter values. In this work, network architectures ranging from 1 to 4 hidden layers and 50 to 200 neurons per hidden layer were tested, and the accuracy and calculation times for each model are shown in Fig. 2. Subplots 2a and 2b show the model accuracy and time per prediction, respectively, plotted against the model architecture. Subplots 2c and 2d show the model accuracy and time per prediction, respectively, plotted against the number of learned parameters in the model. Model accuracy in subplots 2a and 2c is reported as the correlation between the neural network prediction and MMM-predicted data, measured as the R^2 value of a linear regression. Note that the calculation times shown in subplots 2b and 2d came from Python and include the compilation time. They are shown here as a comparison between different model architectures, but should not be taken as the true calculation time for the model. In order to balance the two simultaneous goals of high accuracy and low calculation time, the architecture of 3 hidden layers with 100 neurons per layer was chosen. This architecture displays essentially the same level of accuracy as more complicated architectures, implying that there is enough flexibility for this model to learn the underlying function well. In addition, the calculation time is relatively short compared to architectures which

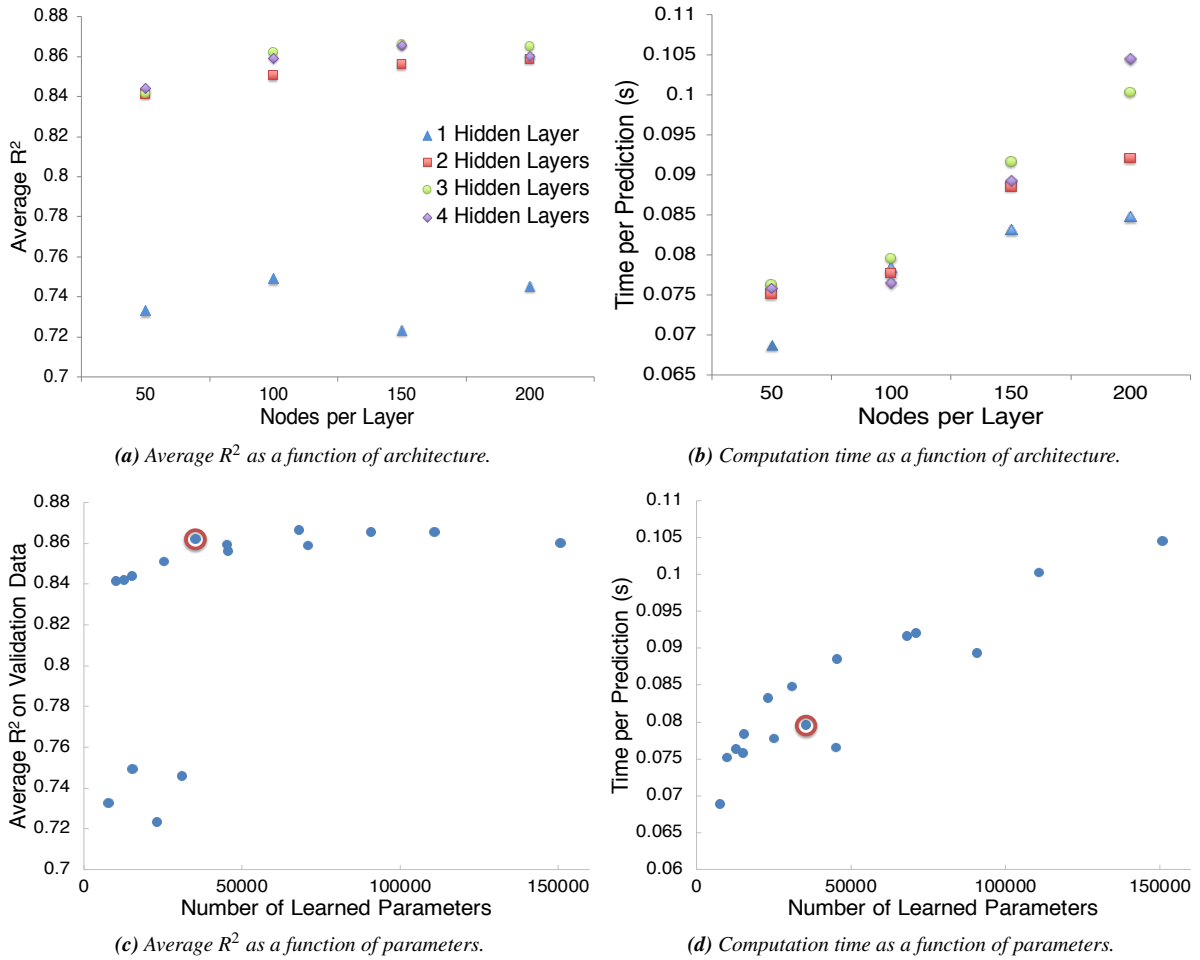


Figure 2: (a) Computation accuracies averaged across all outputs as a function of model architecture (number of layers and nodes per layer), (b) prediction times as a function of model architecture (number of layers and nodes per layer), (c) computation accuracies averaged across all outputs as a function of the number of learned parameters, and (d) prediction times as a function of the number of learned parameters. In plots (c) and (d), the circled values represent 3 hidden layers with 100 nodes per layer, which is the architecture chosen for the final network.

display similar levels of accuracy. The length of the training process was determined in a similar way. The length of the training process is measured in epochs, or number of times that the network sees each data point in the training set during the training process. If training is allowed to run for too long, the network will begin to memorize (overfit) the exact training data instead of learning the underlying function, and the network predictions will not be as accurate on any data point not in the training set. This can be seen in Fig. 3 as the difference in R^2 between the training and validation sets increases with the number of epochs. In order to avoid this issue, training of the final model was limited to 16 epochs.

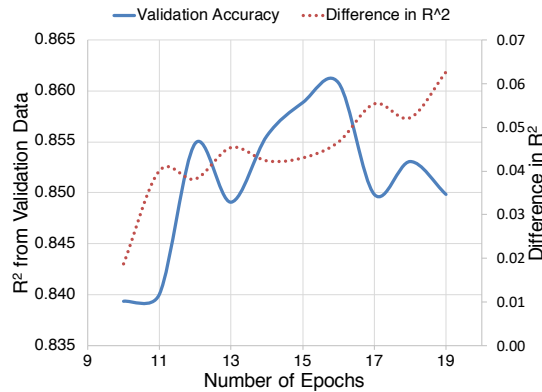


Figure 3: Prediction accuracy on the validation dataset and difference in accuracy between training and validation data vs. number of epochs.

One source of uncertainty in the model stems from the initial randomization of the weights. There is a possibility that, during the training process, the weights are converging to a local minimum of the loss function instead of the global minimum. In order to account for this, five separate models were trained in parallel using the same hyperparameters and the same training data, but different random initial weights. When all five parallel networks converge to the same minimum of the loss function, that is most likely the global minimum. The final network reports the average, standard deviation, minimum, and maximum of the five predictions. If the network is being used for an application that requires even faster calculation times, the user can choose to not use all five parallel networks or to use parallel computing.

4. MODEL EVALUATION

Results of the final neural network model are shown in this section. The correlations between MMM-predicted data and MMMnet predictions for each output on the training and testing datasets are seen in Table 2. Predictions are shown for TRANSP run 176052T05, which is in the testing dataset. Fig 4 shows the evolution of the MMM-predicted data and the MMMnet prediction at the spatial location $\hat{\psi} = 0.612$ over the course of the shot for (a) χ_i , (b) χ_e , and (c) χ_ϕ . Fig. 5 shows the MMM and MMMnet profiles at time $t = 1.82s$ for (a) χ_i , (b) χ_e , and (c) χ_ϕ . The red lines show the MMM-predicted data, the dark blue lines show the average of the five MMMnet predictions, and the blue shaded areas show one standard deviation above and below the average prediction. Note that these plots do not extend all the way to the plasma edge, but cover only the section of the profile that MMMnet predictions are valid for.

Table 2: Correlations (R^2) between MMM and MMMnet predictions for shots in training and testing datasets.

	R^2 values: training data	R^2 values: testing data
χ_i	0.961	0.883
χ_e	0.941	0.843
χ_ϕ	0.928	0.878

In Cython [9], the model takes an average of 1.35 ms to make a prediction per time step. The calculation time has not yet been tested on the DIII-D plasma control system computer, but is expected to be fast enough for real-time control.

5. INTEGRATION INTO COTSIM

COTSIM calculates the electron temperature profile as the numerical solution to the electron heat transport equation [10],

$$\frac{3}{2} \frac{\partial}{\partial t} [n_e T_e] = \frac{1}{\rho_b^2 \hat{H}} \frac{1}{\hat{\rho}} \frac{\partial}{\partial \hat{\rho}} \left[\hat{\rho} \frac{\hat{H}^2}{\hat{F}} \left(\chi_e n_e \frac{\partial T_e}{\partial \hat{\rho}} \right) \right] + Q_e, \quad (1)$$

which is a function of the electron thermal diffusivity χ_e . The electron thermal diffusivity contains both neoclassical and anomalous components, but for the scenarios COTSIM is attempting to simulate the neoclassical component is assumed to be smaller in magnitude than the anomalous component, and is therefore neglected. COTSIM's model library includes multiple options to calculate the anomalous component of χ_e , including the Bohm/gyro-Bohm model [11], the Coppi-Tang model [12], and now MMMnet. Most of the inputs to MMMnet are either already simulated in COTSIM or can be calculated from values already simulated in COTSIM; the few that cannot, such as the fast ion density, are assigned a prescribed value representative of the scenario of interest. A pedestal model [13] is used to calculate the edge of the electron temperature profile. A fixed pedestal width is chosen based on the pedestal width observed in the experiment of interest, and the model is tuned to match the experimental pedestal height. An extrapolation is made for the MMMnet χ_e prediction from the spatial region where MMMnet is valid to the spatial region where the pedestal model is applied.

The results of two COTSIM simulations of shot 147634, one using MMMnet and the other using the Bohm/gyro-Bohm model to predict χ_e , are shown in Fig. 6. The COTSIM results are compared to TRANSP run 147634S01, which is an analysis run and therefore uses the experimental T_e profiles. Note that COTSIM is not expected to perfectly replicate experimental data, partially because a number of simplifying assumptions are used in the calculation of the electron density (n_e) and heating (Q_e) profiles seen in Eq. 1. The COTSIM simulations match each other exactly at the edge because they both use the pedestal model, but both the magnitude and the shape of the T_e profile in the core match the experimental profile much more closely when MMMnet is used.

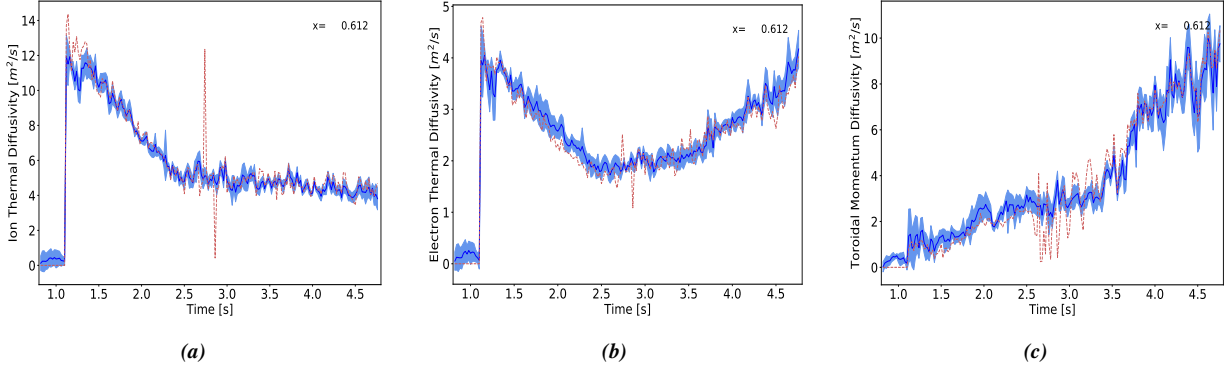


Figure 4: Evolution of a single point ($\hat{\rho} = 0.612$) in the profile over time for (a) χ_i , (b) χ_e , and (c) χ_ϕ . The red lines are the MMM-predicted data, the dark blue lines are the average neural network predictions, and the blue shaded area is one standard deviation above and below the average neural network prediction.

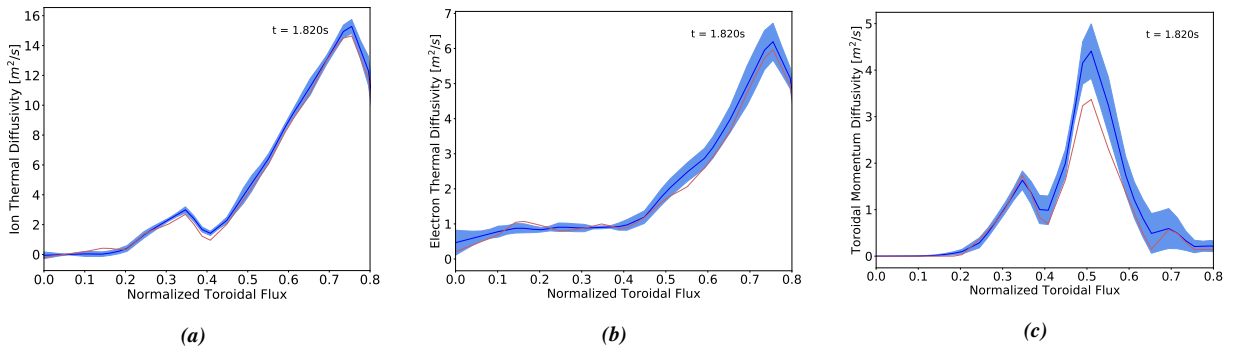


Figure 5: Prediction of the profile at a set time for (a) χ_i , (b) χ_e , and (c) χ_ϕ . The red lines are the MMM-predicted data, the dark blue lines are the average neural network predictions, and the blue shaded area is one standard deviation above and below the average neural network prediction up to normalized toroidal flux of 0.8.

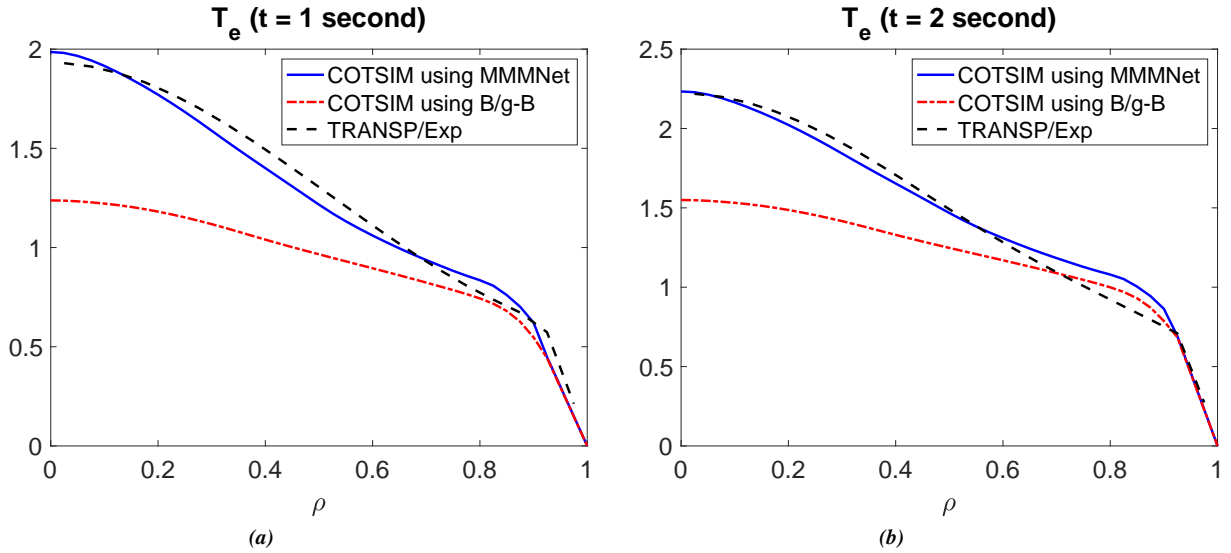


Figure 6: COTSIM prediction of the T_e profile for shot 147634 using χ_e from MMMnet and from the Bohm/gyro-Bohm (B/g-B) model compared to experimental data at (a) $t=1s$ and (b) $t=2s$.

6. CONCLUSIONS AND FUTURE WORK

A neural network version of Multi-Mode Model has been trained to accurately reproduce the results of MMM with a calculation time useful for control applications. A number of improvements to MMMnet are being considered for future work. Other outputs of MMM, including impurity, poloidal momentum, and electron particle diffusivities,

could be included as additional outputs of the neural network. Also, training data could be extended so that the network predictions are valid across the whole spatial domain, from the magnetic axis to the boundary. An enlarged training data set could also extend applicability to an even broader range of plasma scenarios. These improvements would significantly increase the number of applications MMMnet is useful for.

MMMnet has been integrated into COTSIM and used to predict the electron thermal diffusivity. Preliminary results show that the use of MMMnet could produce an electron temperature profile prediction closer in shape to the experimental profile. Future work on COTSIM includes using the MMMnet prediction of χ_ϕ in solving the transport equation for rotation. This step may need to wait until MMMnet can predict diffusivities over the entire spatial domain to avoid issues caused by the current lack of valid diffusivity predictions at the edge of the profile.

ACKNOWLEDGEMENTS

This material is based upon work supported by the U.S. Department of Energy, Office of Science, Office of Fusion Energy Sciences, using the DIII-D National Fusion Facility, a DOE Office of Science user facility, under Awards DE-FC02-04ER54698, DE-SC0010661, DE-SC0013977, and by the National Science Foundation Graduate Research Fellowship Program under Grant No. 1842163.

DISCLAIMER

This report was prepared as an account of work sponsored by an agency of the United States Government. Neither the United States Government nor any agency thereof, nor any of their employees, makes any warranty, express or implied, or assumes any legal liability or responsibility for the accuracy, completeness, or usefulness of any information, apparatus, product, or process disclosed, or represents that its use would not infringe privately owned rights. Reference herein to any specific commercial product, process, or service by trade name, trademark, manufacturer, or otherwise does not necessarily constitute or imply its endorsement, recommendation, or favoring by the United States Government or any agency thereof. The views and opinions of authors expressed herein do not necessarily state or reflect those of the United States Government or any agency thereof.

REFERENCES

- [1] O. MENEGHINI ET AL., Self-consistent core-pedestal transport simulations with neural network accelerated models, *Nucl. Fusion*, **57** (2017)
- [2] J. CITRIN ET AL., Real-time capable first principle based modeling of tokamak turbulent transport, *Nucl. Fusion*, **55** (2015)
- [3] M. BOYER ET AL., Real-time capable modeling of neutral beam injection on NSTX-U using neural networks, *Nucl. Fusion*, **59** (2019)
- [4] S. M. MOROSOHK, M. D. BOYER ET AL., Accelerated version of NUBEAM capabilities in DIII-D using neural networks, *Fusion Eng. Des.*, **163**, 112125 (2021)
- [5] T. RAFIQ, A. KRITZ ET AL., Physics basis of Multi-Model anomalous transport module, *Phys. Plasmas*, **20**, 032506 (2013)
- [6] Lehigh University Plasma Control Group, “COTSIM”, Matlab/Simulink[®] Code
- [7] G.-C. V. P.G. Bernardos, Optimizing feedforward artificial neural network architecture, *Engineering Applications of Artificial Intelligence*, **20**, 365 (2007)
- [8] A. KLEIN, S. FALKNER ET AL., “Fast Bayesian Optimization of Machine Learning Hyperparameters on Large Datasets”, in *Proc. of the 20th International Conference on Artificial Intelligence and Statistics*, volume 54, 528–536, PMLR, Fort Lauderdale, FL, USA (2017)
- [9] S. BEHNEL, R. BRADSHAW ET AL., “C-Extensions for Python”, URL <https://cython.org/>
- [10] V. BASIUK, J. ARTAUD ET AL., Simulations of steady-state scenarios for Tore Supra using the CRONOS code, *Nucl. Fusion*, **43**, 822 (2003)
- [11] M. ERBA, T. ANIEL ET AL., Validation of a new mixed Bohm/gyro-Bohm model for electron and ion heat transport against the ITER, Tore Supra and START database discharges, *Nucl. Fusion*, **38**, 1013 (1998)
- [12] S. JARDIN, M. BELL ET AL., TSC simulation of Ohmic discharges in TFTR, *Nucl. Fusion*, **33**, 371 (1993)
- [13] T. ONJUN, G. BATEMAN ET AL., Models for the pedestal temperature at the edge of H-mode tokamak plasmas, *Phys. Plasmas*, **9**, 5018 (2002)